J Appl Electrochem (2014) 44:1037–1045
DOI 10.1007/s10800-014-0715-x

RESEARCH ARTICLE

$CsHSO_4$ as proton conductor for high-temperature polymer electrolyte membrane fuel cells

Olivia Barron · Huaneng Su · Vladimir Linkov · Bruno G. Pollet · Sivakumar Pasupathi

Received: 29 April 2014 / Accepted: 14 July 2014 / Published online: 17 August 2014

Abstract The influence of $CsHSO_4$ inorganic solid acid was evaluated as a possible proton conductor in the catalyst layer of ABPBI (poly(2,5-benzimidazole))-based high-temperature polymer electrolyte membrane fuel cells (HT-PEMFCs). Gas diffusion electrodes (GDEs) were prepared with fixed polytetrafluoroethylene (PTFE) and polyvinylidene diflouride (PVDF) binder content, while the $CsHSO_4$ loading was varied. Porosimetry data showed that the addition of 10 % $CsHSO_4$ to the PVDF GDE increased the porosity across all the pore regions, whereas the addition of 10 % $CsHSO_4$ to the PTFE GDE decreased the GDEs porosity. The $CsHSO_4$ MEAs showed good proton transfer dynamics and low resistance for fuel cell operation. An optimum loading of 10 % $CsHSO_4$ in conjunction with either of the binders was observed, with $CsHSO_4$–PVDF GDE achieving peak power of 498.2 mW cm^{-2} at a cell voltage of +352 mV. Higher $CsHSO_4$ loadings increased the charge transfer resistance and lowered the cell performance of these GDEs.

Keywords High-temperature polymer electrolyte membrane fuel cell · Catalyst layer · Gas diffusion electrode · Poly(2,5-benzimidazole) · $CsHSO_4$

1 Introduction

Polymer electrolyte membrane fuel cells (PEMFCs) are amongst the most widely studied fuel cells, with the majority of these studies focused on low-temperature (LT) PEMFCs, which in most cases contain perfluorosulphonic acid electrolytes such as Nafion®. Nafion® electrolyte requires water in order to conduct protons, a requirement which necessitates the use of humidified reactant gases and limits operation to temperatures below 100 °C which in turn reduces the overall system efficiency [1]. Higher operational temperatures are expected to result in higher fuel cell performances [2], and as a result and in recent years, there has been a shift in focus from LT-PEMFCs to high-temperature PEMFCs (HT-PEMFCs), which have the capability of operating at temperatures in the range 120–200 °C. HT-PEMFCs offer a number of advantages such as having a higher carbon monoxide (CO) tolerance in the fuel [3], faster electrochemical reaction kinetics, require little or no humidification, faster heat rejection due to the large difference in temperature between the fuel cell and the environment and more useful waste heat. These enable the use of smaller and simpler fuel processing and ancillary systems, which aid in improving the overall efficiency of the fuel cell system. HT-PEMFCs are, however, not without challenges; they should have sufficient heat resistance under zero humidification conditions, and their electrolyte membranes should be capable of chemical coupling with acids that have the ability to conduct protons.

Initially acid-doped PolyBenzImidazole (PBI) membranes that are temperature resistant for operation above 100 °C were investigated by Savinell and coworkers. [4] for their possible use in PEMFCs. These membranes were shown to exhibit good proton conductivity, good mechanical and thermal stability, as well as having a low reactant gas permeability. Weng et al. [5] showed that PBI has a distinct advantage over Nafion®/H_3PO_4 composite electrolytes in that PBI was shown to have an electro-osmotic drag coefficient of nearly zero for temperatures up to

O. Barron · H. Su (✉) · V. Linkov · B. G. Pollet · S. Pasupathi
HySA Systems Competence Centre, South African Institute for Advanced Materials Chemistry, University of the Western Cape, Private Bag X17, Bellville 7535, South Africa
e-mail: suhuaneng@gmail.com

200 °C, whereas the Nafion® composite electrolyte was shown to have an electro-osmotic drag coefficient in the range of 0.2–0.6. This essentially means that when protons are transported through PBI electrolyte, they do not 'drag' water molecules with them, thus ensuring membrane hydration and preventing anode dehydration even at high operating temperatures. The phosphoric acid (PA) used to dope these PBI membranes are often utilised as ionomers in the catalyst layer (CL) of PBI-based HT-PEMFCs [6–8]. More recently, PA-doped poly(2,5-benzimidazole) (AB-PBI) has been shown to have improved proton conductivity over PA-doped PBI, as well as being cheaper to produce since it can be produced from a single commercially available monomer [3,4-diaminobenzoic acid (DABA)] by condensation in polyphosphoric acid (PPA) [9–11]. Theoretically HT-PEMFCs are expected to have improved performance over LT-PEMFCs due to faster reaction kinetics achieved at higher operating temperature; however, this has yet to be achieved mainly due to catalyst deactivation by strong phosphate anion adsorption from the phosphoric acid ionomer onto the platinum (Pt) electrocatalyst, as well as other factors such as the low solubility and diffusivity of oxygen in phosphoric acid [12], catalyst agglomeration and electrochemical carbon corrosion also contribute to the cell performance loss [13, 14].

The above mentioned factors show that there is still a clear need to improve Membrane Electrode Assembly (MEA) of HT-PEMFCs. On the membrane aspect, researchers' efforts have focused on improving the conductivity of the membrane, membrane strength [15–22] and membrane acid retention [18, 23, 24]. While research focus on the GDE has mainly looked at improving the electrocatalyst [25] and reducing the sources of performance degradation for the GDE by optimising both the CL [26–34] and gas diffusion layer (GDL) [28, 35]. The structure and composition of the CL play a critical role in the MEA performance, and in the case of PBI-based MEAs, the CL is composed of the electrocatalyst (typically Pt/C) which catalyses the electrochemical reactions, H_3PO_4 which acts as a proton conductor and facilitates proton transport, as well as a polymer binder to maintain the structural integrity of the CL. The polymer binder influences the structural properties of the electrode; it also maintains the structural integrity which affects mechanical stability and the porosity which in turn influences reactant permeability and catalyst distribution influencing Pt utilisation. All of these factors contribute to the performance of the GDE.

Currently different types of polymer binders such as polytetrafluoroethylene (PTFE), polyvinylidene difluoride (PVDF), polyurethane, PBI, and various other polymers that are capable of incorporating H_3PO_4 into their structure have been utilised in the CL of PBI-based HT-PEMFCs [29, 32, 36]. The aforementioned polymer binders have been studied, and their influence on Pt utilisation has been evaluated [29, 36]; there is, however, a need for an alternative to H_3PO_4 electrolyte in the catalyst layer to improve the low oxygen solubility and the sluggish oxygen reduction reaction (ORR) kinetics and catalyst deactivation occurring due to H_3PO_4 electrolyte [12]. The present study aims to evaluate $CsHSO_4$ as a proton conductor in the CL for HT-PEMFCs and report for the first time (to the best of the authors' knowledge) that an inorganic solid acid such as $CsHSO_4$ can operate at 150–200 °C and undergoes a transformation at approximately 140 °C into a 'superionic' phase and exhibits high conductivity of 10^{-2} S cm^{-1}. From the list of inorganic solid acids that exhibit good proton conductivity at elevated temperature, $CsHSO_4$ was chosen as the best candidate for use in HT-PEMFCs due to its high conductivity in the temperature range of interest to us (160 °C). Solid acids such as CsH_2PO_4 and RbH_2PO_4 exhibit high proton conductivity but in a temperature range that is not suitable for ABPBI-based HT-PEMFCs. $NH_4H_2PO_4$ solid acid exhibits good conductivity in the temperature range of interest, but the phosphate anions would adsorb strongly onto the surface of the Pt electrocatalyst leading to catalyst deactivation [12]. Haile et al. [37] initially demonstrated $CsHSO_4$ as an electrolyte membrane in PEMFCs. Lavrova et al. [38] and Piao et al. [39] showed that $CsHSO_4$ composite electrolyte membranes can be produced with improved stability and conductivity. The effect of $CsHSO_4$, combinations of PTFE–$CsHSO_4$ and PVDF–$CsHSO_4$ on the performance of GDEs was evaluated in ABPBI-based HT-PEMFCs electrochemically by polarisation studies and electrochemical impedance spectroscopy (EIS), and structurally by scanning electrochemical microscopy (SEM) and mercury intrusion porosimetry.

2 Experimental

2.1 Synthesis of $CsHSO_4$ proton conductor

$CsHSO_4$ was synthesised by dissolving 35.3 g of Cs_2SO_4 (Johnson Matthey 99.99 % metals basis) in 200 ml ultrapure water. 21.7 g of H_2SO_4 (Kimix 98 %) was diluted in 50 ml ultrapure water. The diluted H_2SO_4 solution was slowly added drop-wise by a burette to the Cs_2SO_4 solution while heating the Cs_2SO_4 solution to 60 °C and stirring at 250 rpm. The resultant crystals formed were dried overnight at 100 °C. Fourier transform infrared (FT-IR) spectroscopy was used to confirm the formation of $CsHSO_4$.

2.2 Preparation of catalyst ink

HiSpec 4000, 40 wt% Pt/C (Johnson Matthey) was used as the catalyst material for both the anode and cathode CL.

The binders used in the catalyst ink formulation were 60 wt% PTFE emulsion (Electrochem Inc.) and 5 wt% PVDF in DMAc solvent, and the proton conductor used was 40 wt% $CsHSO_4$/aq. solution. The binder and $CsHSO_4$ loadings were normalized in relation to the Pt/C electrocatalyst, with 15 % w/w PVDF and 40 % w/w PTFE binder concentrations used in the catalyst ink formulations. The catalyst ink was prepared by dispersing the electrocatalyst powder with the binder and/-or ionomer in the appropriate solvent of either DMAc (Sigma-Aldrich) or Isopropanol (Johnson Matthey). The catalyst ink mixture was ultrasonicated (40 kHz) for 2 h to disperse the ink before it was used.

2.3 GDE fabrication

An airbrush (Prona) was used to handspray all the prepared GDEs analysed in this study. Commercially available GDL (H2315-CX196, Freudenberg, Germany) was weighed before and after catalyst ink deposition to determine the catalyst loading. The dispersed catalyst ink was deposited in successive layers until the desired amount of catalyst had been deposited, with each layer being dried before the next layer was added. The platinum loading of all anodes and cathodes prepared for this study was 1.0 mg cm^{-2}. The binder content in the CL of these GDEs varies, with some values obtained from literature [6] or optimised by the authors. The GDEs containing only the polymer binders in the CL were cured at 200 °C, and the GDEs containing the $CsHSO_4$ proton conductor as well as the binder-$CsHSO_4$ combinations were cured at 120 °C.

2.4 Single cell test and electrochemical characterisation

Fumapem® AM (Fumatech) ABPBI membrane with a thickness of $\sim$35 µm was used as the electrolyte membrane in this study. Membrane doping was achieved by immersing the membranes in 85 % phosphoric acid (PA) at 95 °C for 24 h. PTFE tape was used as gaskets and together with the doped membrane, was sandwiched between two GDEs and assembled in a single cell fixture (Baltic Fuel Cells GmbH, Germany). The single cell fixture contained two graphite plates with serpentine flow fields with an active area of 5 cm^2. The cell fixture was placed in a Cell Compression Unit (CCU) (Pragma Industries, France) where the cell temperature of 160 °C and piston pressure of 2 N mm^{-2} were maintained during operation. A thermocouple and electrical heaters embedded in the graphite plates enabled the control of the cell by the CCU. Pure hydrogen was supplied to the anode, and air was supplied to the cathode, with flow rates of 0.5 and 1.0 slpm, respectively. With the use of the high flow rates, the mass transport influences on the MEA performance would be minimized, so that the performance based solely on the influence of $CsHSO_4$ can be analysed.

An Arbin BT2000 (Arbin Instruments, USA) was used as an electronic load to evaluate the cells. The MEAs were activated prior to recording the polarisation curves by operating the cell at a constant voltage of 0.55 V until stable performance was achieved. The current–voltage polarisation curves were recorded by measuring the cell voltage as a function of the current. The polarisation curves were measured between open circuit voltage (OCV) and +0.2 V.

EIS was performed using a Potentiostat/Galvanostat (Autolab PGSTAT 302N, Metrohm) equipped with a frequency response analyser (FRA) and a 20 A current booster (Autolab BSTR 20A, Metrohm). EIS measurements were carried out at a cell voltage of +0.6 V, in the 0.1 Hz–20 kHz frequency range with a sinusoidal amplitude of +0.01 V. Autolab Nova software was used to generate and simulate the impedance data.

2.5 Physical characterisation of GDEs

Morphological analysis of the GDEs was carried out by High Resolution Scanning Electron Microscopy (HR-SEM) using a Nova NanoSEM 230, FEI. The pore size distribution of the GDEs was determined by mercury intrusion porosimetry utilising an Auto Pore IV 9500 (Micromeritics) porosimeter.

3 Results and discussion

3.1 Structural analysis

Figure 1a–g shows the HR-SEM micrographs of the GDEs fabricated with binder (PTFE or PVDF) and $CsHSO_4$. The images are taken at 5,000× magnification in Electron BackScatter Diffraction (EBSD) mode so that Pt distribution on the electrode surface can be observed, since high-molecular weight elements, such as Pt, appear much brighter than lower molecular weight elements, e.g. carbon. The inserts are the 50,000x magnification HR-SEM images take in normal detector mode. The effect of using different binders and proton conductors in the CL can be observed from the structural morphology of the electrodes.

At 5,000× magnification, the morphology of the PVDF GDE (Fig. 1a) appears to be significantly different to that of the PTFE GDE (Fig. 1g). The PVDF GDE exhibits a smoother, more uniform distribution, whereas the PTFE GDE appears to have a rougher and more heterogeneous distribution. At 50,000× magnification, the PVDF GDE particles

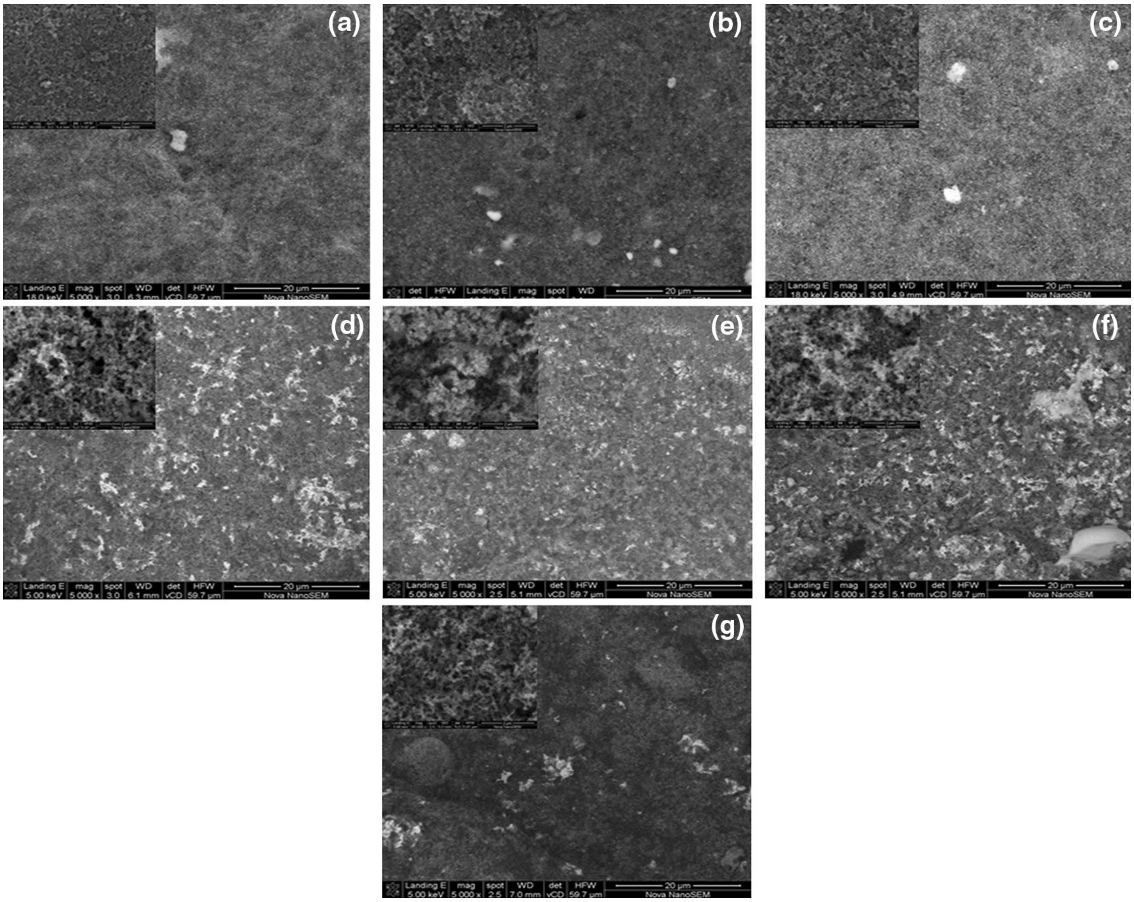

Fig. 1 SEM micrographs showing the surface morphology and porous structure of GDEs prepared with various polymer binders and $CsHSO_4$ proton conductor. **a** PVDF—200 °C; **b** PVDF and 20 % $CsHSO_4$—120 °C; **c** PVDF and 10 % $CsHSO_4$—120 °C; **d** PTFE and 20 % $CsHSO_4$—120 °C; **e** PTFE and 10 % $CsHSO_4$—120 °C; **f** 10 % $CsHSO_4$—120 °C; **g** PTFE—200 °C

appear to be more tightly packed with the consequence that the GDE has less pores when compared to the PTFE GDE, in which the particles are more loosely associated, and the GDE is more porous in nature. The heterogeneous morphology observed in the PTFE GDE may be due to the colloidal nature that PTFE maintains in the catalyst ink which leads to the agglomeration of the catalyst nanoparticles (Fig. 1g). However, in the PVDF electrode (Fig. 1a), this effect is not observed as PVDF remains soluble in the catalyst ink, and agglomeration of the catalyst particles is, hence, less likely to occur. At 5,000× magnification, the surface morphologies of PVDF–$CsHSO_4$ GDEs (Fig. 1b, c) are almost indistinguishable from the PVDF GDE, but at 50,000× magnification, it is possible to discern the effect of the addition of $CsHSO_4$ to the PVDF GDE. The PVDF-$CsHSO_4$ GDEs have particles that are more loosely packed than the PVDF GDE, with these PVDF–$CsHSO_4$ GDEs showing a more porous morphology than the PVDF GDE. In Fig. 1d, e the effect of the addition of $CsHSO_4$ to the PTFE GDE can be observed on the surface of the electrode, in that the Pt catalyst particles appear to form larger clusters than the GDEs prepared with the PVDF and PTFE binder (Fig. 1a, g), which may result from the impaired 'binding' effect of the polymer binders due to the existence of the inorganic particles. At 50,000× magnification, the GDEs (Fig. 1d–g) the morphologies of the GDEs are nearly indistinguishable from each other with the exception of the PTFE-20 % $CsHSO_4$ GDE (Fig. 1d) in which we observe slightly larger pores.

The $CsHSO_4$ electrode (Fig. 1f) also shows a good Pt distribution, but with less uniform surface than that of the PVDF electrode (Fig. 1a) which can be attributed to the 'binding' effect, the PVDF polymer has on the CL, a property which $CsHSO_4$ lacks. For this reason, the $CsHSO_4$ was used together with PVDF and PTFE binders, and the effect this addition had on the surface morphology of the GDEs can be observed in Fig. 1b–e, showing a smoother and more uniform layer than $CsHSO_4$ GDEs alone (Fig. 1f).

Figure 2 shows the mercury intrusion porosimetry results obtained for the PTFE GDE, PVDF GDE as well as the binder-$CsHSO_4$ GDEs. The cumulative intrusion graph shows distinct differences between the PTFE, PVDF and

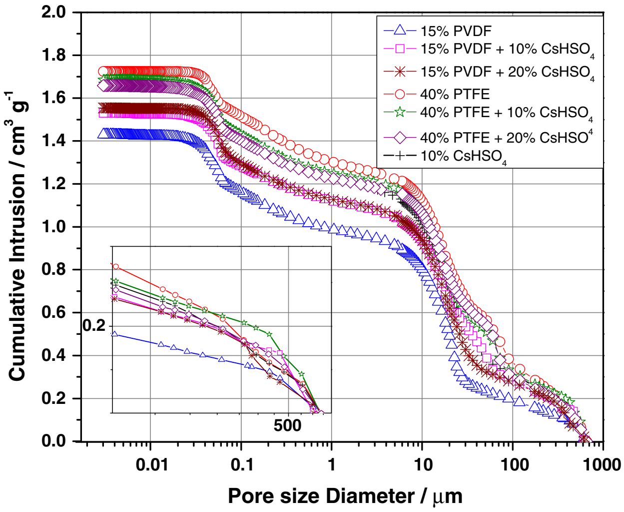

Fig. 2 Cumulative intrusion of the GDEs with various polymer binders and $CsHSO_4$ in the CL

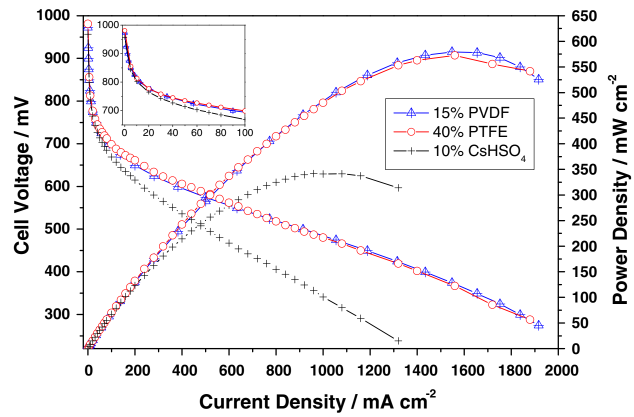

Fig. 3 Polarisation and power density curves for the MEAs with different polymer binders and $CsHSO_4$ proton conductor

binder-$CsHSO_4$ GDEs. The PVDF GDE has the fewest pores and is clearly the least porous of all the GDEs; these results are confirmed by the SEM images (Fig. 1a). Addition of $CsHSO_4$ to the PVDF GDE effectively increased the number of pores and the pore size across all regions. The PVDF-$CsHSO_4$ GDEs exhibit similar porous structures except in the 20–60 µm macropore range, where the PVDF-10 % $CsHSO_4$ GDE contains a larger number of pores in this region.

The opposite effect is observed in the PTFE GDE, where the addition of $CsHSO_4$ has the effect of decreasing the pore volume of the GDE across almost the entire pore range except in the 300–600 µm range, with the PTFE–$CsHSO_4$ GDEs which have a larger pore volume in this region which can be seen in the inset. Pore diameters >100 µm are more likely due to cracks on the GDE surface.

These results are understandable considering that although $CsHSO_4$ is hygroscopic, the PTFE binder is hydrophobic, and they may in essence cancel each other out. However, PTFE is insoluble in the catalyst ink, so large catalyst agglomerates are more likely to form, which would justify the larger macropore volume of the electrodes with CL containing PTFE and/or $CsHSO_4$ ingredients.

In the case of gas transport to the catalyst sites, the main contribution to gas transport will primarily be due to *Knudsen diffusion* in the micropores and a molecular diffusion mechanism in the macropores [40]. Better mass transport would be expected for the electrodes with larger volume of the macropores.

3.2 Electrochemical Analysis

Figure 3 shows the polarisation and power density curves for a single cell HT-PEMFC with PTFE, PVDF and $CsHSO_4$ in the CL. The results indicate that the MEAs with polymer binders show far greater performance than the MEA with the $CsHSO_4$ proton conductor in the CL. At peak power, the MEA fabricated with the PVDF binder exhibits up to 69 % higher power compared to the $CsHSO_4$ MEA. This substantial difference can be attributed to the difference in the GDEs morphology, with the $CsHSO_4$ lacking a 'binding' capability in the CL, with a consequential lack of structural stability in the $CsHSO_4$ GDE. The PTFE and PVDF MEAs exhibit nearly identical performance, with the PTFE MEA achieving maximum power density of 572.52 mW cm^{-2} at 367 mV and the PVDF MEA reaching a maximum power density of 579.58 mW cm^{-2} at 374 mV. At a cell voltage of +0.6 V, the PTFE MEA reaches a higher current density of ~440 mA cm^{-2}, which is almost 15 % higher than the PVDF MEA which has a current density of ~382 mA cm^{-2} at the same cell voltage. Even though the PTFE and PVDF GDEs exhibit distinctly different porosity data, a larger number of macropores as exhibited by the PTFE GDEs should result in better mass transport than the PVDF GDE which has fewer macropores, but these two MEAs exhibit nearly identical performance. The EBSD HR-SEM images of the PVDF GDE shown in Fig. 1a shows a better Pt catalyst distribution to the PTFE GDE (Fig. 1g), which could result in improved Pt utilisation and result in a performance comparable to a GDE with better porosity. The $CsHSO_4$ MEA has the lowest current density of 240 mA cm^{-2} at the same cell voltage and is ~45 and 37 % lower than the PTFE and PVDF MEAs, respectively.

The inset in Fig. 3 is the enlarged polarisation curve of the low current density region (<100 mA cm^{-2}). Closer examination of this region indicates that the initial voltage drop is the smallest for the PTFE GDE and highest for the $CsHSO_4$ GDE (PTFE < PVDF < $CsHSO_4$). Since this region of the curve is determined by activation overpotential, which is largely controlled by the sluggish kinetics of the ORR, it can be assumed that the PTFE GDE has the faster reaction kinetics. The curves of the PTFE and PVDF MEAs are nearly identical in the linear region, indicating that these MEAs should exhibit similar ohmic resistances, whereas the $CsHSO_4$ MEA shows a polarisation curve with a much steeper slope in the linear region, indicating that the ohmic resistance for this GDE is greater than that of the PVDF and PTFE GDEs. We postulate that the $CsHSO_4$ electrode lacks the structural integrity provided by the polymer network of the binders, leading to an increase in contact resistance. As expected, the high-current density (>1,000 mA cm^{-2}) region of the polarisation curves displays no sharp drop from the ohmic region of the curves, indicating that these MEAs are not significantly influenced by mass transport limitations due to the high gases flow rates. From the point of view of commercialization and real applications, usage of low stoichiometric gases is more practical to operate PEM fuel cells. In this case, an increase in mass transport limitation could be expected, but it would not be serious due to the absence of liquid water under this high operating temperature (160 °C), which will be investigated in our further work.

A combination of the different binders and $CsHSO_4$ proton conductor in the CL was tested to evaluate whether the binder-proton conductor configuration improved the performance of the MEAs. Figure 4a, b shows the polarisation and power density curves for the MEAs with different binders and $CsHSO_4$ proton conductor in the CL, respectively. At a working cell voltage of +0.6 V, the maximum current density is achieved by the PTFE MEA, with the PVDF-20 % $CsHSO_4$ MEA exhibiting the lowest current density of 150 mA cm^{-2} at the same cell voltage. From the polarisation curves, we observe a decrease in current density at +0.6 V that follows the following trend: PTFE > PVDF > PVDF-10 % $CsHSO_4$ > PTFE-10 % $CsHSO_4$ > $CsHSO_4$ > PTFE-20 % $CsHSO_4$ > PVDF-20 % $CsHSO_4$. An enlarged image of the low current density region in Fig. 4a is shown in the inset. The results show that the addition of the binders to the 10 % $CsHSO_4$ GDE results in a smaller voltage drop when compared to the $CsHSO_4$ GDE, indicating that the addition of the binders improved the electrode kinetics of the $CsHSO_4$ GDE.

The binder-20 % $CsHSO_4$ MEAs exhibited the lowest performance of all the MEAs, indicating that higher $CsHSO_4$ loadings in the CL are not beneficial. Clearly, the lower amount (10 %) $CsHSO_4$ combination with either polymer binder produces the better performance. Figure 4b shows that the PVDF-10 % $CsHSO_4$ MEA achieved the highest peak power of the binder-$CsHSO_4$ MEAs reaching a maximum power density of 492.8 mW cm^{-2} at a cell voltage of +352 mV, which is nearly twice the value of 250 mW cm^{-2} at 350 mV achieved by Wannek et al. [6] with Pt loadings of ~1 mg cm^{-2} Pt and 40 % PTFE in the catalyst layer. However, it should be mentioned that Wannek et al. used low stoichiometric flow rates for MEA testing, so the performance in their work could be further enhanced if same gas flow rates were used as in this work. Nevertheless, higher gas flow rates should not give much improvement in the performance because the mass transport limitation of high-temperature PEMFC depends on the gas flow rates limitedly due to the absent of liquid water in the catalyst layers. Therefore, the results in this work are still considered to be comparable with the performances reported in the literature.

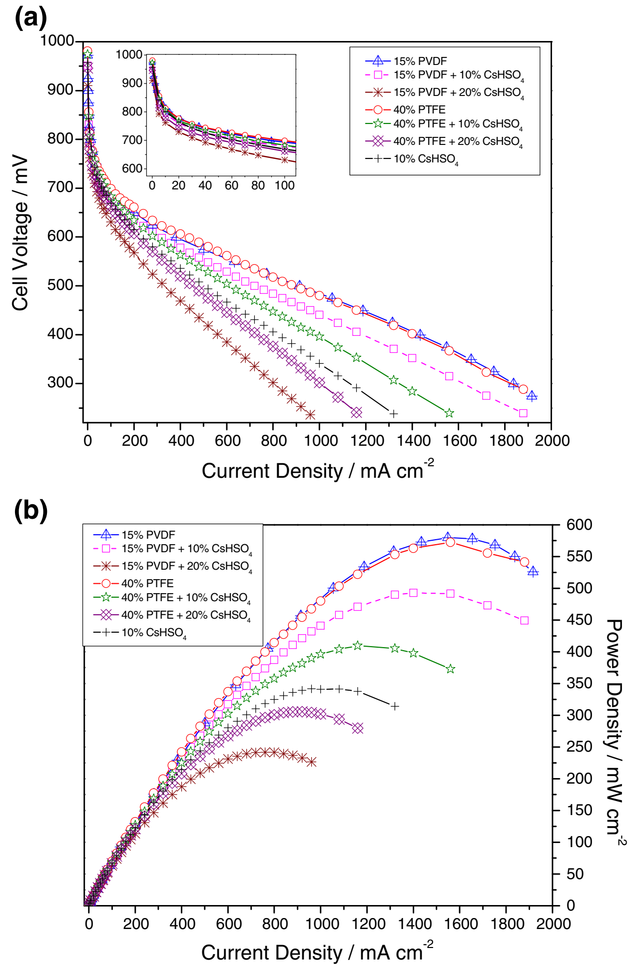

Fig. 4 **a** Polarisation curves of the MEAs with different polymer binders and/-or proton conductor in the CL of the GDEs. **b** Power density curves of the MEAs with different polymer binders and/-or proton conductor in the CL of the GDEs

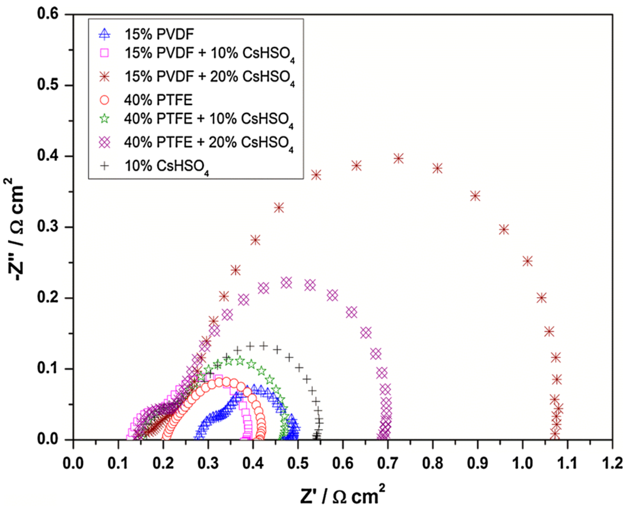

Fig. 5 In situ impedance spectra of the MEAs with different polymer binders and $CsHSO_4$ at a cell voltage of 0.6 V

Table 1 Impedance and *Tafel slope* characteristics of the MEAs

GDE	% Binder and/-or proton conductor	Tafel slope (mV dec^{-1})	R_{Ω} (mΩ cm^{-2})	R_{CT} (mΩ cm^{-2})
PTFE	40 %	91.4	208	208
PTFE–$CsHSO_4$	40 % PTFE-10 % $CsHSO_4$	92.4	152	316
	40 % PTFE-20 % $CsHSO_4$	91.68	145	546
PVDF	15 %	104.99	280	208
PVDF–$CsHSO_4$	15 % PVDF-10 % $CsHSO_4$	91.68	131	255
	15 % PVDF-20 % $CsHSO_4$	87.47	146	926
$CsHSO_4$	10 %	98.03	168	374

Although the PTFE MEA exhibits nearly identical performance to the PVDF MEA when only the binders are used in the CL, the PVDF binder used in conjunction with 10 % CsHSO4 exhibits a peak power that is ~20 % higher than when PTFE binder is used in conjunction with 10 % $CsHSO_4$, the PVDF binder clearly poses the best choice for use with the $CsHSO_4$ in the CL.

In order to obtain more information about the electrochemical characteristics of the GDEs prepared with the PTFE, PVDF binders and the $CsHSO_4$ inorganic solid acid, AC impedance was performed in situ under the same operating conditions at a cell voltage of +0.6 V. Figure 5 shows the impedance spectra of the MEAs with the various binders and proton conductor in the CL of the GDEs. The total ohmic resistance, R_{Ω}, of the cell can be obtained from the high-frequency intercept of the real axis, and the R_{CT} can be estimated from the diameter of the low-frequency and high-frequency intercept.

Table 1 shows the results from measured impedance spectra as well as the *Tafel slopes* for the various MEAs. From the impedance spectra in Fig. 5, it can be seen that there is no significant difference in R_{Ω}, with the exception of the PTFE and PVDF MEAs, since the R_{Ω} represents the total ohmic resistance of the cell which is made up of the contact resistance between the cell components and the ohmic resistance of the membrane, catalyst layer, gas diffusion layer, and bipolar plates [41]. The only differences in the MEAs are the composition of the catalyst layers; one may therefore conclude that the catalyst layer of the PTFE GDE has a much lower ohmic resistance, which if we refer to Fig. 1g can be attributed to the lower interfacial contact resistance provided by the PTFE GDE which has a more irregular surface with catalyst agglomerates that can lead to improved interfacial contact resistance due to the flexibility of the membrane and the cell assembly pressure exerted on the MEA [32]. This morphology is not observed in the PVDF GDE (Fig. 1a) and could be the reason for the higher ohmic resistance seen here.

Nevertheless, it is clear that the MEAs containing $CsHSO_4$ as proton conductor in the CLs have lower R_{Ω} values than those for the MEAs with the polymer binder (i.e. PVDF GDE and PTFE GDE), this lower R_{Ω} in the $CsHSO_4$ MEAs can be attributed to the increased proton transfer in the CLs resulting from the use of the proton conductor, consequently the lower proton transport resistance. It has been reported that the proton transport resistance in the CL causes a 45° (degree)-straight line at the high-frequency region of the first arc [42], which can also be observed in this current study (Fig. 5), proving that the addition of $CsHSO_4$ proton conductor in the CL lowers the proton transport resistance. Another possible reason for the higher R_{Ω} values for the PTFE and PVDF MEAs could be due to the membrane conductivity; although it is assumed that the membrane should have the same PA doping if the same membrane doping procedure is followed, subtle differences in the same membrane can result in different membrane conductivities.

The lowest R_{CT} of 208 mΩ cm^{-2} was achieved by the MEAs with the PVDF GDE as well as the PTFE GDE which indicates that these GDEs have the more efficient electrochemical active layer. These R_{CT} values confirm the results seen in the polarisation and power density curves (Fig. 4a, b). The lowest R_{CT} of the MEAs with the binder-proton conductor configuration was achieved by the PVDF-

10 % $CsHSO_4$ MEA which has a R_{CT} value of 255 mΩ cm^{-2}.

The PVDF-10 % $CsHSO_4$ MEA exhibits a much lower charge transfer resistance than the 10 % $CsHSO_4$ only MEA, suggesting that the addition of the polymer binder to the CL of the $CsHsO_4$ GDE improves the kinetics of the ORR in the catalyst layer of the GDE, this finding corresponds to the increased performance observed in Fig. 4. The *Tafel slopes* shown in Table 1 were estimated from fitting the experimental data (not shown) to

$$E_{iR-\mathrm{Free}} = a + b\log(\mathrm{i}),$$

where $E_{iR\text{-Free}}$ is the iR free voltage of the low current density region of the polarisation curve, a is a constant, and b is the Tafel slope. The *Tafel slopes* for the MEAs with the combination of the polymer binders and proton conductor were all in the range of 87–93 mV dec^{-1} which is well below the value of 120 mV dec^{-1} obtained for phosphoric acid fuel cells (PAFCs), and since the *Tafel slope* provides information on the kinetics of the ORR, it can be stated that in the case of the PVDF GDE, the addition of $CsHSO_4$ proton conductor improves the ORR kinetics in these electrodes. The addition of $CsHSO_4$ to the PVDF MEAs improved the *Tafel slope* values and lowered ohmic resistance of these MEAs, whereas in the case of the PTFE MEAs, the addition of $CsHSO_4$ did not improve the *Tafel slope* values but also lowered the ohmic resistance of these MEAs. The binder-$CsHSO_4$ MEAs exhibit higher charge transfer resistance values to the binder GDEs as well as exhibiting lower performance. The advantages of the improved *Tafel slope* values in the PVDF-$CsHSO_4$ MEAs as well as the lower ohmic resistance values for both binder-$CsHSO_4$ MEAs are clearly negated by the higher charge transfer resistance of these MEAs. The lower performance exhibited by the binder-$CsHSO_4$ MEAs indicates that although the polymer binders improved the stability of the $CsHSO_4$ proton conductor in the CL, the resistance of $CsHSO_4$ to fuel cell environment still needs further improvement.

4 Conclusions

Composite GDEs were constructed using $CsHSO_4$ as the proton conductor and PVDF/PTFE as the polymer binder in the CL. The electrochemical analysis indicated that MEAs prepared with $CsHSO_4$ in the CL can efficiently lower the proton transfer resistance. However, the MEAs prepared solely using $CsHSO_4$ in the CL exhibited lower performance (341.76 mW cm^{-2} at 356 mV) than the MEAs prepared from GDEs using the polymer binders, possibly due to the hygroscopic nature of $CsHSO_4$ which absorbed moisture from the atmosphere during the air-spraying procedure and caused incomplete formation of the pore structure in the CL. The performance and R_{CT} of the $CsHSO_4$ GDEs were improved by addition of a polymer binder to the CL. The $CsHSO_4$ MEA provided the best performance when used in conjunction with a 15 % PVDF binder, enabling the 15 % PVDF–10 % $CsHSO_4$ MEA to achieve a maximum power density of 492.8 mW cm^{-2} at 352 mV, further improvement in the single cell performance can be expected by further optimization of the binder and $CsHSO_4$ contents in the CL. Since $CsHSO_4$ inorganic solid acid is conductive in the 140–200 °C range, an operating temperature higher than 160 °C may prove be beneficial in improving the performance of the MEAs based on these binder-$CsHSO_4$ GDEs, but this temperature is higher than 160 °C operating temperature which we have found optimum for the ABPBI membrane.

Acknowledgments This work is supported by Hydrogen and Fuel Cell Technologies RDI Programme (HySA), funded by the Department of Science and Technology in South Africa, project KP1S01.

References

1. Freire T, Gonzalez ER (2001) Effect of membrane characteristics and humidification conditions on the impedance response of polymer electrolyte membrane fuel cells. J Electroanal Chem 503:57–68
2. Oono Y, Fukuda T, Sounai A, Hori M (2010) Influence of operating temperature on cell performance and endurance of high temperature proton exchange membrane fuel cells. J Power Sour 195:1007–1014
3. Krishnan P, Park J-S, Kim C-S (2006) Performance of a poly(2,5-benzimidazole) membrane based high temperature PEM fuel cell in the presence of carbon monoxide. J Power Sour 159(2):817–823
4. Wainright JS, Wang JT, Weng D, Savinell RF, Litt M (1995) Acid-doped polybenzimidazoles: a new polymer electrolyte. J Electrochem Soc 142(7):L121–L123
5. Weng D, Wainright JS, Landau U, Savinell RF (1996) Electro-osmotic drag coefficient of water and methanol in polymer electrolytes at elevated temperatures. J Electrochem Soc 143(4):1260–1263
6. Wannek C, Lehnert W, Mergel J (2009) Membrane electrode assemblies for high-temperature polymer electrolyte fuel cells based on poly(2,5-benzimidazole) membranes with phosphoric acid impregnation via the catalyst layers. J Power Sour 192(2):258–266
7. Kwon K, Kim TY, Yoo DY, Hong S-G, Park JO (2009) Maximization of high-temperature proton exchange membrane fuel cell performance with the optimum distribution of phosphoric acid. J Power Sour 188(2):463–467
8. Wang J-T, Savinell RF, Wainright J, Litt M, Yu H (1996) A H_2/O_2 fuel cell using acid doped polybenzimidazole as polymer electrolyte. Electrochim Acta 41(2):193–197
9. Linares JJ, Sánches C, Paganin VA, González ER (2011) Poly(2,5-benzimidazole) membranes: physico-chemical characterization and high temperature PEMFC application. In: 11th polymer electrolyte fuel cell symposium, PEFC 11–220th ECS Meeting, Boston. pp 1579–1593
10. Asensio J (2004) Proton-conducting membranes based on poly(2,5-benzimidazole) (ABPBI) and phosphoric acid prepared by direct acid casting. J Membr Sci 241(1):89–93

11. Asensio J, Gómez-Romero P (2005) Recent developments on proton conducting poly(2,5-benzimidazole) (ABPBI) membrane for high temperature polymer electrolyte membrane fuel cells. Fuel Cells 5(3):336–343
12. Qingfeng L, Hjuler HA, Bjerrum NJ (2000) Oxygen reduction on carbon supported platinum catalysts in high temperature polymer electrolytes. Electrochim Acta 45:4219–4226
13. Lobato J, Cañizares P, Rodrigo MA, Linares JJ (2007) PBI-based polymer electrolyte membranes fuel cells Temperature effects on cell performance and catalyst stability. Electrochim Acta 52(12):3910–3920
14. Oh H-S, Lee J-H, Kim H (2012) Electrochemical carbon corrosion in high temperature proton exchange membrane fuel cells. Int J Hydrogen Energy 37(14):10844–10849
15. Angioni S, Righetti PP, Quartarone E, Dilena E, Mustarelli P, Magistris A (2011) Novel aryloxy-polybenzimidazoles as proton conducting membranes for high temperature PEMFCs. Int J Hydrogen Energy 36(12):7174–7182
16. Asensio JA, Borrós S, Gómez-Romero P (2003) Enhanced conductivity in polyanion-containing polybenzimidazoles. Improved materials for proton-exchange membranes and PEM fuel cells. Electrochem Commun 5(11):967–972
17. Carollo A, Quartarone E, Tomasi C, Mustarelli P, Belotti F, Magistris A, Maestroni F, Parachini M, Garlaschelli L, Righetti PP (2006) Developments of new proton conducting membranes based on different polybenzimidazole structures for fuel cells applications. J Power Sour 160(1):175–180
18. Lobato J, Cañizares P, Rodrigo MA, Úbeda D, Pinar FJ (2011) Enhancement of the fuel cell performance of a high temperature proton exchange membrane fuel cell running with titanium composite polybenzimidazole-based membranes. J Power Sour 196:8265–8271
19. Kumbharkar SC, Islam MN, Potrekar RA, Kharul UK (2009) Variation in acid moiety of polybenzimidazoles: investigation of physico-chemical properties towards their applicability as proton exchange and gas separation membrane materials. Polymer 50(6):1403–1413
20. Li M, Scott K (2010) A polymer electrolyte membrane for high temperature fuel cells to fit vehicle applications. Electrochim Acta 55(6):2123–2128
21. Wang RF, Liao SJ, Fu ZY, Ji S (2008) Platinum free ternary electrocatalysts prepared via organic colloidal method for oxygen reduction. Electrochem Commun 10(4):523–526
22. Hasiotis C, Deimede V, Kontoyannis C (2001) New polymer electrolytes based on blends of sulfonated polysulfones with polybenzimidazole. Electrochim Acta 46:2401–2406
23. Pinar FJ, Cañizares P, Rodrigo MA, Ubeda D, Lobato J (2012) Titanium composite PBI-based membranes for high temperature polymer electrolyte membrane fuel cells. Effect on titanium dioxide amount. RSC Adv 2(4):1547
24. Linares JJ, Sanches C, Paganin VA, Gonzalez ER (2012) Poly(2,5-bibenzimidazole) membranes: physico-chemical characterization focused on fuel cell applications. J Electrochem Soc 159(7):F194–F202
25. Fujigaya T, Okamoto M, Nakashima N (2009) Design of an assembly of pyridine-containing polybenzimidazole, carbon nanotubes and Pt nanoparticles for a fuel cell electrocatalyst with a high electrochemically active surface area. Carbon 47(14):3227–3232
26. Jin YC, Okada M, Hibino T (2011) A comparative study of Pt/C cathodes in Sn0.9In0.1P2O7 and H3PO4 ionomers for high-temperature proton exchange membrane fuel cells. J Power Sour 196(11):4905–4910
27. Li H, Liao SJ (2009) Preparation of large Co nanosheets with enhanced coercivity by a magnetic-field-assisted solvothermal approach free of surfactants, complexants or templates. J Magn Magn Mater 321(17):2566–2570
28. Pan C, Li Q, Jensen JO, He R, Cleemann LN, Nilsson MS, Bjerrum NJ, Zeng Q (2007) Preparation and operation of gas diffusion electrodes for high-temperature proton exchange membrane fuel cells. J Power Sour 172(1):278–286
29. Mazúr P, Soukop J, Paidar M, Bouzek K (2011) Gas diffusion electrodes for high temperature PEM type fuel cells-role of a polymer binder and method of the catalyst layer deposition. J Appl Electrochem 41:1013–1019
30. Lobato J, Cañizares P, Rodrigo MA, Linares JJ, Pinar FJ (2010) Study of the influence of the amount of PBI–H_3PO_4 in the catalytic layer of a high temperature PEMFC. Int J Hydrogen Energy 35(3):1347–1355
31. Oono Y, Sounai A, Hori M (2009) Influence of the phosphoric acid-doping level in a polybenzimidazole membrane on the cell performance of high-temperature proton exchange membrane fuel cells. J Power Sour 189(2):943–949
32. Su H, Pasupathi S, Bladergroen B, Linkov V, Pollet BG (2013) Optimization of gas diffusion electrode for polybenzimidazole-based high temperature proton exchange membrane fuel cell: evaluation of polymer binders in catalyst layer. Int J Hydrogen Energy 38(26):11370–11378
33. Felix C, Jao T-C, Pasupathi S, Pollet BG (2013) Optimisation of electrophoretic deposition parameters for gas diffusion electrodes in high temperature polymer electrolyte membrane fuel cells. J Power Sour 243:40–47
34. Higuchi E, Okamoto K, Miyatake K, Uchida H, Watanabe M (2006) Gas diffusion electrodes for polymer electrolyte fuel cell using sulfonated polyimide. Res Chem Intermed 32(5–6):533–542
35. Lobato J, Cañizares P, Rodrigo MA, Úbeda D, Pinar FJ, Linares JJ (2010) Optimisation of the microporous layer for a polybenzimidazole-based high temperature PEMFC. Effect of carbon content. Fuel Cells 10(5):770
36. Park JO, Kwon K, Cho MD, Hong S-G, Kim TY, Yoo DY (2011) Role of binders in high temperature PEMFC electrode. J Electrochem Soc 158(6):B675–B681
37. Haile SM, Boysen DA, Chisholm C, Merle RB (2001) Solid acids as fuel cell electrolytes. Nature 410:910–913
38. Lavrova G, Russkih M, Ponomareva V, Uvarov N (2006) Intermediate-temperature fuel cell based on the proton-conducting composite membranes. Solid State Ion 177(19–25):2129–2132
39. Piao J, Liao S, Liang Z (2009) A novel cesium hydrogen sulfate–zeolite inorganic composite electrolyte membrane for polymer electrolyte membrane fuel cell application. J Power Sour 193(2):483–487
40. Lee H-K, Park J-H, Kim D-Y, Lee T-H (2004) A study on the characteristics of the diffusion layer thickness and porosity of the PEMFC. J Power Sour 131(1–2):200–206
41. Yuan X, Wang H, Colinsun J, Zhang J (2007) AC impedance technique in PEM fuel cell diagnosis—a review. Int J Hydrogen Energy 32(17):4365–4380
42. Kim J-R, Yi JS, Song T-W (2012) Investigation of degradation mechanisms of a high-temperature polymer-electrolyte-membrane fuel cell stack by electrochemical impedance spectroscopy. J Power Sour 220:54–64